Degenerate phase-conjugate four-wave mixing in a nearly-Doppler-free two-level atomic medium

Binh Do
Department of Physics and School of Electrical and Computer Engineering, Purdue University, West Lafayette, Indiana 47907

Jongwhan Cha and D. S. Elliott
School of Electrical and Computer Engineering, Purdue University, West Lafayette, Indiana 47907

S. J. Smith
JILA, University of Colorado and the National Institute for Standards and Technology, Boulder, Colorado 80309
(Received 26 May 1998)

We present experimental observations of phase-conjugate degenerate four-wave mixing in a two-level atomic system (the $3s\,^2S_{1/2}$, $F=2$, $m_F=2\rightarrow 3p\,^2P_{3/2}$, $F=3$, $m_F=3$ transition in a diffuse, collision-free, thermal beam of atomic sodium) driven by cw, narrow-band ($\sim$250 kHz), stabilized pump and probe fields. The primary measurements that we report are of the peak signal strength of the four-wave-mixing interaction and the bandwidth of the four-wave-mixing spectrum (as the laser frequency is tuned through the resonant frequency) as a function of the intensity of the pump field. We compare these measurements with the predictions of a theoretical analysis in which extension to include the effect of the small transverse velocity ($\sim$3 m/sec) of the atomic beam is critical. These measurements provide a direct verification of the theory of this important nonlinear interaction. [S1050-2947(98)06010-7]

PACS number(s): 42.50.Gy, 32.80.−t, 42.65.Hw

I. INTRODUCTION

Phase-conjugate four-wave mixing (FWM) has been studied in scores of atomic, molecular, and condensed phase media, and has found useful application in a variety of related fields. Perhaps the most intriguing application of the general process of phase conjugation is related to its ability to reverse the wave fronts of an incident beam, providing the basis for an exotic mirror [1]. Such a phase-conjugate mirror can be used to remove wave-front distortions of a beam, thus improving the quality of an image or decreasing the minimum spot size of a focused beam. A phase-conjugate mirror can also be used in an optical resonator by replacing a conventional mirror, thereby making the cavity less sensitive to distortions caused by imperfect optical elements within the cavity [2]. Its potential for determining spatial convolutions and image correlations has been explored [3,4], as has its application as a narrow-band optical filter [5]. The spectral width of the FWM spectrum is Doppler free, allowing for high-resolution spectroscopic determinations [6–8]. Due to its high sensitivity, it has been exploited for detection of dilute species [9–12] and determination of temperature from rotational and vibrational spectra of molecules [13]. Self-pumped oscillators based on FWM have also been explored [14–18]. Slusher *et al.* [19] used nondegenerate FWM in a cavity to generate squeezed states of radiation.

With all this activity centered around phase-conjugate four-wave mixing, it is surprising that there has been no measurement of this important interaction taken under conditions that closely match those of the fundamental theory by Abrams and Lind [20,21]. Ideally, these conditions would include (1) a nonlinear medium that is well described as a closed, two-level system, (2) a medium in which inhomogeneous broadening effects (e.g., Doppler broadening) are negligible, (3) a collision-free environment, and (4) excitation of the medium by a laser field that is cw and narrow band. In this paper we report our observations of phase-conjugate four-wave mixing in an experimental configuration in which conditions (1), (3), and (4) are realized, and condition (2) is approximately satisfied. We measure the peak signal strength of this field, as well as the bandwidth of the interaction, and observe good quantitative agreement with the theory for this interaction, providing we include the effect of the Doppler shift due to the transverse velocity component of our atomic beam geometry. Our initial interest in this interaction derives from related studies [22] we have carried out on the role of the coherence of the laser on this coherent interaction. In order to understand measurements of these laser coherence effects, we have worked to minimize the complexity of the system as much as possible.

A schematic representation of the geometry of the phase-conjugate degenerate four-wave mixing experiment is shown in Fig. 1. Forward and backward pump beams propagate exactly antiparallel to one another, and a weak probe field is incident in a direction making a small angle θ with respect to the forward pump beam. These input fields are all at the same frequency, ω_L. The interaction with the nonlinear medium produces a fourth field, also at the frequency ω_L, which propagates back on the incident probe beam. This field is called the phase conjugate field since it can be shown that its wave fronts are exactly reversed from those of the

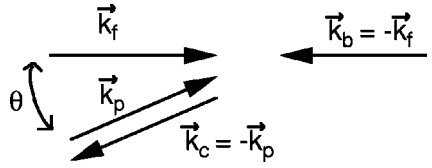

FIG. 1. Schematic representation of the four optical beams present in phase-conjugate four-wave mixing.

probe field. In terms of complex field amplitudes, this is equivalent to saying that the field generated through the nonlinear interaction is proportional to the complex conjugate of the field amplitude of the probe beam.

In 1978, Abrams and Lind [20] presented a theoretical description of phase-conjugate four-wave mixing in an ensemble of two-level atoms, but only for the stationary atom case. Their density matrix formulation was valid for arbitrary intensity of the forward and backward pump beams, I_f and I_b, respectively. We consider only the case in which the lower state of the two-level system is the ground state of the atom and there is no population of the upper state before the pump and probe beams are turned on, conditions which are satisfied in our experiment. We also limit our discussion to the case of a weakly absorbing medium of atomic density N and length L, for which the expression Abrams and Lind found for the phase-conjugate reflectivity, $R=I_c/I_p$ (I_c and I_p are the intensities of the phase-conjugate and probe beams, respectively), of the medium reduces to $|\beta L|^2$, where

$$\beta=\alpha_0\frac{1}{i-\Delta/\gamma_{12}}\frac{2(I_fI_b)^{1/2}/I_{\rm sat}}{\{[1+(I_f+I_b)/I_{\rm sat}]^2-4I_fI_b/I_{\rm sat}^2\}^{3/2}}, \tag{1}$$

and α_0 is the weak-field absorption coefficient,

$$\alpha_0=\frac{\omega_L N}{2nc}\frac{|\mu_{12}|^2}{\hbar\epsilon_0\gamma_{12}}. \tag{2}$$

$I_{\rm sat}$ is the saturation intensity of the transition,

$$I_{\rm sat}=\frac{1}{2}\epsilon_0 c\frac{\hbar^2\gamma_{12}\Gamma_0}{|\mu_{12}|^2}[1+(\Delta/\gamma_{12})^2]=I_{\rm sat}^0[1+(\Delta/\gamma_{12})^2], \tag{3}$$

γ_{12} is the transverse relaxation rate, Γ_0 is the population decay rate, μ_{12} is the transition dipole moment, Δ is the detuning of the laser frequency from the resonant frequency of the transition, and $I_{\rm sat}^0$ is the saturation intensity at $\Delta=0$. For the case where the forward and backward pump intensities are equal, $I_f=I_b$, we can use the frequency dependence of $I_{\rm sat}$ as given in Eq. (3) to show

$$|\beta L|^2=\left(2\alpha_0 L\frac{I_f}{I_{\rm sat}^0}\right)^2\left\{\frac{\gamma_{12}^2}{\Delta^2+\gamma_{12}^2(1+4I_f/I_{\rm sat}^0)}\right\}^3. \tag{4}$$

At low intensities, $I_f\ll I_{\rm sat}$, the FWM interaction is second-order in the pump field, resulting in a reflectivity that increases as I_f^2. At high intensities, $I_f\gg I_{\rm sat}$, the reflectivity decreases as I_f^{-1}, as saturation of the atomic response limits the contributing dipoles to those near the nodes of the standing-wave pattern of the optical electric field. With the pump intensity greater than $I_{\rm sat}$, the volume of unsaturated atoms surrounding the nodes decreases in size, allowing fewer atoms to radiate into the phase-conjugate field. In Refs. [20,21], the maximum FWM signal occurs at $I_f=I_{\rm sat}/2$, at which intensity one can show that the phase-conjugate reflectivity is $R=(\alpha_0 L)^2/27$. Using Eqs. (3) and (1), one can also show that the width of this four-wave mixing response as the laser frequency is tuned through resonance frequency is given by

$$\Delta\omega_{\rm FWM}=2\gamma_{12}\sqrt{(\sqrt[3]{2}-1)(1+4I_f/I_{\rm sat}^0)}. \tag{5}$$

The importance of the transverse velocity of the atoms or molecules has long been recognized [6,9,21,23–29]. The atomic motion effectively tunes the frequency of the input beams and the FWM beam out of resonance with the atomic transition. Thus the forward pump and probe are red shifted if $\vec{k}_f\cdot\vec{v}>0$, (where $\vec{k}_f$ is the propagation vector of the forward pump beam, $\vec{v}$ is the atomic velocity, and the crossing angle between the forward pump and probe, θ, is small) while the backward pump and phase conjugate beams are blueshifted. Resonance enhancement of this highly nonlinear interaction is essential if the atoms are to contribute to the FWM signal, but we can see that the Doppler shift precludes this enhancement for any atoms with $|\vec{k}_f\cdot\vec{v}|>\Gamma_0$ for any laser frequency. With only the zero-transverse-velocity atoms taking part, the linewidth of the FWM spectrum is limited to a value close to the homogeneous linewidth (including, for example, the natural linewidth, collisional broadening, and power broadening) of the transition. By this qualitative argument, we can understand that the frequency width of the FWM response of a Doppler-broadened vapor is much smaller than the Doppler width of the transition. A quantitative analysis of the effect of the atomic motion on the FWM interaction, however, is a difficult problem. We find it necessary to include atomic motion in the analysis of our measurements, even though our medium is an atomic beam with only a small transverse velocity component.

The outline of the paper is as follows. We will discuss our measurements in detail in the next section, and follow with a discussion of the experimental results. We develop a theoretical explanation of these results in Sec. IV, and give a summary of our conclusions in Sec. V.

II. EXPERIMENT

In this section, we discuss our experiment in detail. Our primary objectives in setting up the experimental configuration were to establish and maintain a closed, collision-free, two-level atomic system with minimal Doppler broadening, to use narrow-band, stabilized pump and probe beams, and to assure uniform intensity of the pump beam in the interaction region. We chose atomic sodium in a beam geometry as our nonlinear medium for this work. As an alkali metal, the spectroscopy of sodium is relatively simple and well characterized. It has a conveniently high vapor pressure, making it relatively easy to generate an atomic beam. While its nuclear spin leads to a complex hyperfine structure [30], this is easily overcome using standard optical pumping techniques [31], allowing us to produce a true closed, two-level atomic system. We tune the circularly polarized laser field to the $3s\,^2S_{1/2}$, $F=2\rightarrow 3p\,^2P_{3/2}$, $F=3$ transition frequency. The $3s\,^2S_{1/2}$, $F=2$, $m_F=2$ state and the $3p\,^2P_{3/2}$, $F=3$, $m_F=3$ state constitute a closed two-level system in that the right-circularly polarized light can couple these states only to each other, and the upper state can decay spontaneously only

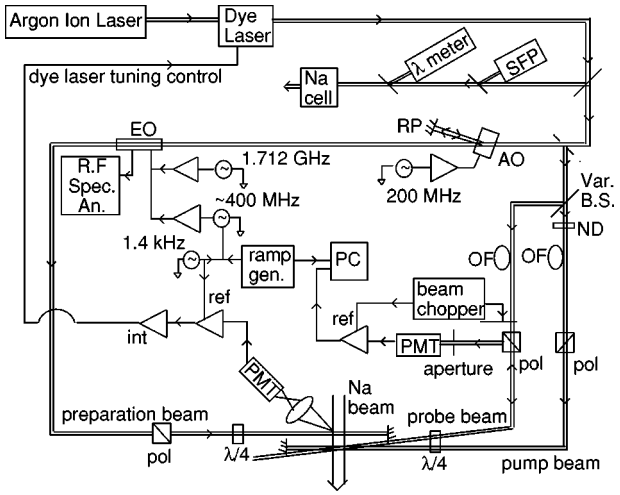

FIG. 2. Schematic diagram of the experiment. Abbreviations in this diagram are used for the scanning Fabry-Pérot interferometer (SFP), the acousto-optic modulator (AO), the electro-optic modulator (EO), a roof prism (RP), optical fibers (OF), photomultipliers (PMT), a personal computer (PC), polarizers (pol), and quarter-wave retarders ($\lambda/4$).

to the lower. The saturation intensity for this transition is $I^0_{\rm sat}=6.33$ mW cm^{-2}.

The sodium atomic beam is generated using a single-chamber, stainless steel effusive oven, typically run at 300 °C. The opening in the oven through which the atoms escape has a diameter of 2 mm. A second aperture, whose diameter is also 2 mm, is placed 40 cm from the oven. The beam size in the interaction region (10 cm beyond the second aperture) is defined by these two apertures. We calculate the average velocity of the atoms to be 9.1×10^4 cm/sec, with a transverse velocity distribution whose width (full width at half maximum, FWHM) is 300 cm/sec. The density of the atomic beam in the interaction region, as determined by the temperature of the oven, the size of the oven nozzle, and the distance to the interaction region [32], is 2.7×10^8 cm^{-3}. At the operating temperature of our oven, the vapor pressure of diatomic sodium [33] is about 1% that of monatomic sodium. The background pressure in the interaction region is 5×10^{-6} torr.

A schematic diagram of the experiment, emphasizing the optical and electronic implementation of the laser frequency control, is shown in Fig. 2. An argon ion laser operating on all lines pumps a cw, frequency-stabilized, tunable dye laser. The dye laser produces 230 mW at 589.0 nm, and its frequency is stabilized by locking to an external hermetically sealed reference cavity. When locked, the laser has a residual linewidth of 200–300 kHz and power fluctuations of about 2–3% of the average output power. The laser is capable of maintaining single-mode operation while being tuned over a frequency range of tens of GHz, and will typically stay locked to the reference cavity for 0.5–2.0 h.

A few mW of the main beam is split off to facilitate monitoring and adjustment of the laser. The laser mode structure is monitored using a scanning confocal Fabry-Pérot optical spectrum analyzer (SFP) with a 2-GHz free spectral range. We tune the laser to within 10 GHz of the $D2$ transition in atomic sodium using a home-made wavemeter, and to within 1.5 GHz by observing the fluorescence in a heated glass sodium vapor cell.

Next, the main laser beam is split into three components: the preparation beam, the pump beam, and the probe beam. The pump and probe beams drive the FWM interaction, while the preparation beam transfers the atoms into a single hyperfine component of the ground state, helps to collimate the atomic beam, and provides an error signal with which we control the detuning of the pump and probe field frequency with respect to the resonant frequency of the sodium. The preparation beam is phase modulated in a $LiTaO_3$ electro-optic crystal (EO). The modulation signal consists of two frequency components, $\nu_{m1}\sim400$ MHz, and $\nu_{m2}=1.712$ GHz. This produces sidebands on the optical carrier (at the optical frequency, ν_0) at the two modulation frequencies, ν_{m1} and ν_{m2}, as well as at mixing frequencies, $\pm m\nu_{m1}\pm l\nu_{m2}$, where m and l are any positive integers. We convert the polarization of the preparation beam to circular using a quarter-wave Fresnel rhomb ($\lambda/4$). The preparation beam crosses the atomic beam at right angles, and is reflected back on itself after exiting the vacuum chamber. With the laser beam diameter of ~0.5 cm and a peak intensity of 150 mW cm$^{-2}=25I^0_{\rm sat}$ in the pumping sideband, the atoms undergo the cycling transition ~150 times in the time they travel through the preparation beam.

The laser frequency is stabilized using the Pound-Drever scheme [34,35], as follows. We collect the fluorescence from the intersection between the preparation beam and the atomic beam with a 1-in focal length lens onto a 1P28 photomultiplier (PMT). We impose a dither frequency of 1.4 kHz on the ν_{m1} sideband, and detect the amplitude modulation of the PMT signal at the dither frequency to generate an error signal, which, when integrated, we use to correct the laser frequency ν_0. Locking with this scheme assures the condition $\nu_{21}=\nu_0+\nu_{m1}$, where ν_{21} is the resonance frequency of the sodium transition. The second-order sideband of the preparation beam at the frequency $\nu_0+\nu_{m1}+\nu_{m2}$ is resonant with the $3s\,^2S_{1/2},\ F=1\rightarrow3p\,^2P_{3/2},\ F=2$ transition, and has the task of recovering ground-state atoms that otherwise would be trapped in the $F=1$ hyperfine level. This it does quite effectively, as we see that the FWM signal is approximately doubled when this sideband is turned on.

Finally, we are able to improve the collimation of the atomic beam by tuning the preparation beam a few MHz to the red side of the transition frequency. We believe this to be evidence of a transverse cooling mechanism [36,37]. The width of the absorption spectrum of the sodium beam (natural linewidth ~10 MHz) when the preparation beam is resonant with the transition is ~16 MHz, but when tuned to the red side of the transition it is ~13 MHz, and when tuned to the blue side of the transition, ~30 MHz.

The beam from which the pump and probe beams are derived is separated from the preparation beam by diffracting the former twice (in a double pass configuration) in a 200-MHz acousto-optic modulator (AO). By virtue of this double-diffraction scheme, the pump and probe frequency will always be $\nu_L=\nu_0+400$ MHz. Since we lock the laser frequency to the transition frequency, ν_{21}, such that $\nu_{21}=\nu_0+\nu_{m1}$, the detuning of the pump and probe beams from resonance is also controlled, $\Delta/2\pi\equiv\nu_L-\nu_{21}=400$ MHz $-\nu_{m1}$. The pump and probe beams are separated from one

another in a variable beam splitter, with ~ 40 μW power in the probe beam and 15 mW in the pump beam. The pump power is varied using a neutral density filter wheel (ND). We focus the pump and probe beams into single-mode optical fibers to clean up the transverse mode structure and to minimize any displacement of the beams in the interaction region. We actively stabilize the power of the probe beam using an acousto-optic modulator (not shown in Fig. 2) as a variable attenuator, driven by an error signal produced with a photodiode-amplifier-integrator network. Each beam is linearly polarized in separate polarizing cubes, and directed into the vacuum chamber. Before entering the vacuum, they pass through a common quarter-wave retarder (a zero-order birefringent wave plate), which circularly polarizes the input pump and probe beams. We mechanically chop the probe beam at a frequency of ~ 160 Hz to allow phase-sensitive detection of the FWM signal.

In the interaction region, we cross the pump and probe fields with the atomic beam at right angles to minimize the Doppler-broadening effects. The pump beam and probe beam are collimated and nearly parallel to one another, crossing at an angle of $\theta \sim 10$ mrad. We minimize this angle as much as possible, with the constraint that the beams must be spatially separated at the windows of the vacuum system so that scattered light from the pump beam does not mask the signal beam. The beam radius (defined as the radius at which the intensity drops to e^{-2} of its on-axis intensity) of the pump beam (1.42 mm) is 4 times larger than that of the probe beam (0.34 mm), assuring that as the beams cross in the interaction region, the intensity of the pump beam is uniform to within 15% where the probe intersects it. We measure the pump power by comparison with a callibrated (1%) photodetector. It is also important that the beam diameters be large enough to limit transit time effects. An average-velocity atom takes 1.5 μsec to travel through the pump beam, and 0.37 μsec to travel through the probe beam. Both these times are significantly greater than the transverse relaxation time of sodium, $T_2 = 32$ nsec, and so exert no significant influence on the FWM spectrum.

The backward pump beam is produced by reflecting the forward pump beam back on itself after it leaves the vacuum chamber. The transmission of each of the antireflection-coated windows on the vacuum system is ~ 0.985, so that $I_b = 0.97 I_f$, justifying our approximation that the forward and backward pump beams are of nearly equal intensity. We estimate that the angle between the forward and backward pump beams is equal to π $(180°)$ to within 0.1 mrad. This alignment is important so that the phase-conjugate wave is phase matched with the nonlinear polarization of the atomic medium. Quantitatively, one can show that phase matching is acheived when $|\Delta\vec{k}|L \ll 1$, where $\Delta\vec{k} = \vec{k}_f + \vec{k}_b - \vec{k}_p - \vec{k}_c$, and L is the length of the medium. For the geometry of our experiment, the alignment angle of the pump beams must be much less than $\lambda/(2\pi L\theta) = 2$ mrad. We test the polarization of the pump beam by observing the transmission of the backward pump beam by the linear pump-beam polarizer. Misalignment of the quarter-wave plate or birefringence of the optical windows of the vacuum chamber would alter the polarization of the pump beams, and would be detected as an increase (from the ideal value of zero) in the transmission by the pump-beam polarizer. We test the quality of the probe-beam polarization in a similar fashion, reflecting the probe beam back on itself and observing the transmission of the backward-reflected probe beam by the probe-beam polarizer. For both the pump and probe beams, we observe the transmission by the polarizers to be insignificant.

We measure the weak-field absorption spectrum of the sodium beam in order to monitor the alignment of the laser beams, the alignment of the magnetic dipoles, the collimation of the atomic beam, and the density of the atomic beam. The atomic beam crosses the preparation beam ~ 2 cm before the atoms reach the interaction region. Using three sets of orthogonal magnetic field coils, we cancel the Earth's magnetic field to within 10 mG, and impose a field of about 0.5 G along the direction of propagation of the pump field. The absorption spectrum shows no detectable absorption at the frequency of the $3s\,^2S_{1/2}$, $F=2 \rightarrow 3p\,^2P_{3/2}$, $F=2$ transition frequency, 60 MHz lower than the $3s\,^2S_{1/2}$, $F=2 \rightarrow 3p\,^2P_{3/2}$, $F=3$ transition frequency, verifying that the sodium is effectively pumped into the $F=2$, $m_F=2$ component of the ground state, and that the alignment of the magnetic dipoles is maintained as the atoms travel to the interaction region.

The width of the absorption spectrum is typically 12.5 to 14.5 MHz, only slightly larger than the 10-MHz natural linewidth of the transition. We determine the width of the velocity distribution, $g(v)$, of the atomic beam by fitting the absorption spectrum to a Voight profile,

$$\frac{\Delta I(\omega)}{I} \propto \int \mathcal{L}(\omega_{12} - \vec{k}\cdot\vec{v}, \Gamma) g(v)\, dv, \tag{6}$$

where, $\mathcal{L}(\omega_{12} - \vec{k}\cdot\vec{v}, \Gamma)$ represents a Doppler-shifted Lorentzian line-shape function of width Γ, and $g(v)$ is the probability distribution of the transverse velocities. We assume a Gaussian shape for $g(v)$,

$$g(v) = \sqrt{\frac{4\ln(2)}{\pi}} \frac{1}{\Delta v} \exp\left[-4\ln(2) \left(\frac{v}{\Delta v} \right)^2 \right], \tag{7}$$

where Δv is the width (FWHM) of the transverse velocity distribution of the atomic beam, and adjust Δv to minimize the sum of the squares of the deviation between the measured absorption spectrum and the fit. For a 12.5-MHz absorption width, as we measured for the absorption spectrum taken with the FWM data presented in this work, we find that Δv is 280 cm/sec, translating to a Doppler width of 5 MHz. This agrees with our estimate of the transverse velocity width based solely upon the geometric arguments (size of the apertures that define the atomic beam and their spacing) and the average thermal energy of the sodium atoms. Finally, we measure a peak absorption of the probe beam by the sodium beam of $\sim 12\%$, corresponding to $\alpha_0 L = 0.0625$. This is in reasonable agreement with our estimate of $N\sigma_{\text{abs}} L/2 = 0.067$, where N was given earlier, $\sigma_{\text{abs}} \simeq (g_1/g_2)\lambda^2/2\pi = 1.66 \times 10^{-9}$ cm^2 is the absorption cross section, $g_1 = 1$ and $g_2 = 3$ are the degeneracies of the lower and upper levels, respectively, and $L \simeq 3$ mm.

The phase-conjugate beam generated through the nonlinear action of the atoms propagates counter to the direction of the incident probe beam. After passing back through the quarter-wave retarder, which circularly polarizes the input pump and probe beams, the conjugate beam is linearly po-

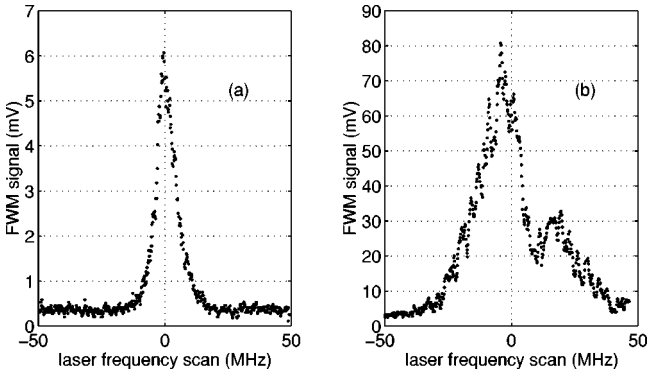

FIG. 3. Two-sample FWM spectra. In (a), the pump intensity is $0.10I^0_{\rm sat}$, while in (b) it is $8.0I^0_{\rm sat}$.

larized, with its polarization axis orthogonal to that of the probe. The polarizer cube (pol) then reflects the phase-conjugate beam toward a photomultiplier, which we use to detect the power of this beam. An aperture (1 mm diameter) in front of the PMT is necessary to reduce the level of background light that would otherwise reach the PMT and mask the phase-conjugate signal. This light arises predominantly from scattering of the pump beam from the window in the vacuum chamber. These windows are AR coated to reduce losses, but scattering due to imperfections could still easily obscure the signal. The PMT output is amplified in a lock-in amplifier, with the reference input (at $\sim$160 Hz) to the lock-in amplifier being generated by the controller for the beam chopper of the probe beam. We have calibrated this detection system by attenuating the probe beam with neutral density filters, and reflecting the probe into the PMT. This allows absolute measurement of the FWM optical power, by measuring the reflected probe power with a calibrated (1%) photodetector. The output of the lock-in amplifier is recorded by a laboratory PC using an external analog-to-digital converter, which concurrently records the scan voltage used to tune the $\sim 400-$MHz sideband (which then indirectly tunes the laser frequency). We calibrate the nearly linear frequency scan by monitoring the sideband frequency on a rf spectrum analyzer.

III. RESULTS

For each pump-laser power, we scan the pump and probe frequency together through the resonance frequency, and record the power of the phase-conjugate signal as a function of the optical frequency. Two typical spectra are shown in Fig. 3. The intensities of the pump beam for these two spectra are $0.10I^0_{\rm sat}$ and $8.0I^0_{\rm sat}$. Overall, we measured FWM spectra at 20 different pump intensities ranging from $0.10I^0_{\rm sat}$ to $12I^0_{\rm sat}$. The intensity of the probe beam is held constant at $0.17I^0_{\rm sat}$ (2 μW power). At this probe intensity, we measure that the phase-conjugate signal is linear in the probe power. Consistent with the Abrams and Lind theory [20,21], we observe that the phase-conjugate signal initially increases with increasing pump power until the intensity of the pump beam approaches $I^0_{\rm sat}$. Further increase in the pump intensity results in a decrease in the phase-conjugate signal.

The FWM spectra that we observe are generally in good agreement with what we expect. There are two important features to these spectra that must be carefully noted. First, we consistently observe a strong dip in the signal when the pump and probe frequency is greater than the resonant frequency of the atoms. We attribute this dip to transverse heating by the pump beam, through which the atoms must travel before they reach the probe beam. This effect is the same as that which we described in our discussion of the preparation beam. With the pump laser tuned to the blue side of resonance, the population of low transverse velocity atoms remaining in the atomic beam in the interaction region is significantly decreased. The phase-conjugate signal is extremely sensitive to the transverse velocity of the atoms, as we will discuss in the next section. We expect that the FWM spectrum is probably enhanced by transverse velocity cooling with the pump tuned to the red side of the resonance, but this effect is minimal since the atomic beam is already well collimated.

In addition, we observe a small asymmetry in our FWM spectra. This asymmetry is independent of the rate or direction of the scan of the laser frequency. We believe that the asymmetry is likely due to the finite bandwidth of the laser. We will discuss this asymmetry further in a future paper [22].

To analyze the data, we fit the measured phase-conjugate signal to the expression

$$P_{\rm FWM}=\frac{P_0}{[(\nu_L-\nu_{21})^2+(\Delta\nu_{\rm FWM}/2)^2]^3}+S. \qquad (8)$$

We adjust the peak height P_0, the center frequency ν_{21}, the width of the spectrum, $\Delta\nu_{\rm FWM}$, and the dc offset S to determine the least-squares deviation between the data and the fit. For pump intensities greater than the saturation intensity the blue-side dip may make it difficult to accurately determine the best fit to these spectra. For these curves we exclude a portion of the measured spectra from the fit, using only the data up to line center and the data in the extreme blue wing where we believe the heating effect is minimal. The asymmetry that we observe in the low-intensity spectra, however, is undoubtedly present in the high-intensity data as well, so the accuracy of this method is limited. None the less, this method of estimating the peak height and width is reasonably consistent with measurements we take directly from the traces of the spectra with pencil and ruler. Where necessary, we expand the estimated uncertainties on our results for these spectra to account for any differences.

In Fig. 4 we plot the magnitude of the phase-conjugate reflectivity (the phase-conjugate power divided by the probe power) and the width of the phase-conjugate spectrum as a function of the pump intensity. The solid line in each figure is the result of the Abrams and Lind theory, given in Eqs. (4) and (5), while the diamonds represent the experimental data. While the general shape of the experimental curve for the reflectivity matches that predicted by theory, we see that at low intensities the phase-conjugate intensity is well below the theoretical curve. The pump laser intensity that yields the maximum phase-conjugate intensity is larger than the predicted value of $I^0_{\rm sat}/2$ by more than a factor of three. The widths of the spectra are in good agreement with the theoretical expectations, except at small pump intensities where the minimum linewidth that we measure is around 8 MHz, larger than the 5-MHz linewidth expected on the basis of Eq.

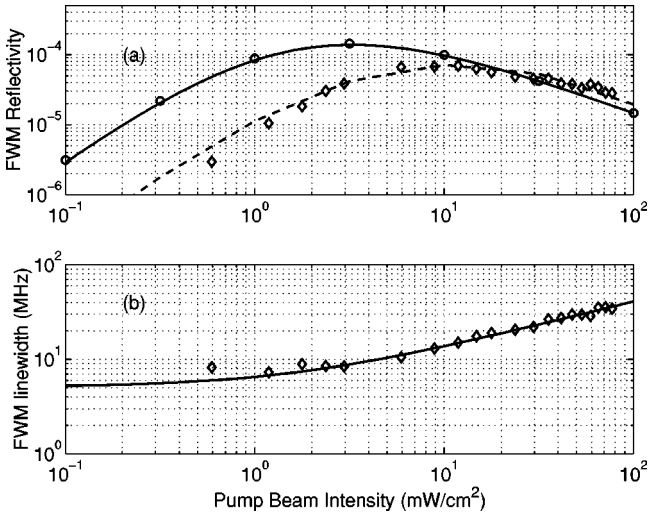

FIG. 4. FWM reflectivity (a) and FWM linewidth (b) vs the intensity of the pump beam. The solid line is from Refs. [20,21], and the diamonds are the experimental data points. The uncertainties in the data points are smaller than or comparable to the dimensions of the diamonds. Our numerical results are shown as the circles (for stationary atoms) and as the dashed line (for moving atoms).

(5). As we shall see in the next section, this deviation with the theory can be explained by the small amount of residual Doppler broadening present in our atomic beam geometry. The solid lines in Fig. 4 are valid for stationary atoms. In light of the relatively small magnitude of the Doppler distribution, we find it surprising that it has such a significant impact on the data shown in Fig. 4. Our calculations show, however, that at low intensities only a small fraction of the atoms, those whose transverse velocity is sufficiently low, contribute to the phase-conjugate signal. As the intensity increases, the atomic response is power broadened and more atoms are able to contribute. This shifts the saturation of the signal to higher intensities.

IV. THEORY

In this section, we discuss the theory of the nonlinear interaction of a two-level quantum system with a laser field that leads to the phase-conjugate four-wave-mixing signal, explicitly including the effect of atomic motion. In our approach, we write the components of the Bloch vector as a Fourier expansion in the phase factor of the probe beam, for which we can determine the amplitudes through a direct numerical integration of the optical Bloch equations. This technique is similar to that used in Ref. [26] in which the authors calculated the FWM signal in a Doppler-broadened three- and four-level system. We can evaluate these elements for arbitrary field strength of the pump laser or probe laser, and we can easily separate the terms that are properly phase matched to radiate in the direction of the signal beam. The result of this analysis is a determination of the phase-conjugate reflectivity, allowing for the transverse velocity of the atomic beam, which we use for direct quantitative comparison with our experimental results.

The interaction of the laser field with the atomic system can be calculated by writing the Hamiltonian of the system as

$$H = H^0 + V(\vec{r},t), \tag{9}$$

where H^0 represents the atomic Hamiltonian, and $V(\vec{r},t)$ is the interaction Hamiltonian between the laser field and the two-level system. The components of the interaction energy matrix are $V_{ij} = -\vec{\mu}_{ij}\cdot\vec{\mathcal{E}}(\vec{r},t)$, where $\vec{\mu} = e\vec{r}$ is the transition electric dipole moment, and $\vec{\mathcal{E}}(\vec{r},t)$ is the total field incident upon the medium,

$$\begin{aligned}\vec{\mathcal{E}}(\vec{r},t) &= \hat{\epsilon}\{E_f\cos(\vec{k}_f\cdot\vec{r}-\omega_L t) + E_b\cos(-\vec{k}_f\cdot\vec{r}-\omega_L t) \\ &\quad + E_p\cos(\vec{k}_p\cdot\vec{r}-\omega_L t)\} \\ &= \frac{1}{2}\{\vec{E}(\vec{r},t)e^{-i\omega_L t} + \vec{E}^*(\vec{r},t)e^{i\omega_L t}\},\end{aligned} \tag{10}$$

where

$$\vec{E}(\vec{r},t) = \hat{\epsilon}\{E_f e^{i\vec{k}_f\cdot\vec{r}} + E_b e^{-i\vec{k}_f\cdot\vec{r}} + E_p e^{i\vec{k}_p\cdot\vec{r}}\}. \tag{11}$$

As indicated by these equations, we use two counterpropagating pump fields propagating in the direction $\vec{k}_f$ and $\vec{k}_b = -\vec{k}_f$, and a weak probe beam propagating in a direction $\vec{k}_p$. All three beams are degenerate at a frequency ω_L. The polarization of the laser field is given by $\hat{\epsilon}$, and $\vec{E}^*(\vec{r},t)$ is the complex conjugate of the field amplitude $\vec{E}(\vec{r},t)$. The forward and backward pump beams form a standing-wave pattern in the medium, and are of nearly the same intensity. We will let $E_b = E_f$ in our analysis. The temporal evolution of the system is described by the equations of motion of the density matrix,

$$\dot{\rho}_{21} = \left(\frac{\partial}{\partial t} + \vec{v}\cdot\vec{\nabla}\right)\rho_{21} = -i\omega_{21}\rho_{21} - \frac{i}{\hbar}V_{21}(\rho_{11}-\rho_{22}) - \frac{\rho_{21}}{T_2}, \tag{12}$$

$$\dot{\rho}_{11} = \left(\frac{\partial}{\partial t} + \vec{v}\cdot\vec{\nabla}\right)\rho_{11} = -\frac{i}{\hbar}\{V_{12}\rho_{21} - V_{21}\rho_{12}\} + \frac{\rho_{22}}{T_1}$$

where the diagonal elements of the density matrix represent the population probability distribution between the two atomic levels, and the off-diagonal elements include the complex oscillatory dipole moment, i.e., the coherence, of the system. The coherence terms are related by $\rho_{21} = \rho_{12}^*$, and for a closed system such as the one we are considering, the population is conserved, i.e., $\rho_{11} + \rho_{22} = 1$. The energy difference between the atomic states is $\hbar\omega_{21} = \hbar(\omega_2 - \omega_1) = h\nu_{21}$. The final terms in these equations represent the decay of the population of the upper state (with lifetime $T_1 = \Gamma_0^{-1}$) and of the coherence (with lifetime $T_2 = \gamma_{12}^{-1}$). The elements of the density matrix are a strong function of position and velocity because of the standing-wave pattern created by the counterpropagating pump beams.

The standard approach [38] to simplify the spatial and temporal derivatives in these equations of motion is to transform to the rest frame of the atom, $\vec{r} \rightarrow \vec{r} + \vec{v}t$, so that the field amplitude becomes

$$\vec{E}(\vec{r},t)=\hat{\epsilon}\{E_f e^{i\vec{k}_f\cdot(\vec{r}+\vec{v}t)}+E_b e^{-i\vec{k}_f\cdot(\vec{r}+\vec{v}t)}+E_p e^{i\vec{k}_p\cdot(\vec{r}+\vec{v}t)}\}. \tag{13}$$

Moving into a rotating frame through the substitution $\rho_{21}=\sigma_{21}e^{-i\omega t}$ and $\rho_{ii}=\sigma_{ii}$ and keeping only the terms that evolve at frequencies much less than optical frequencies allows one to write

$$\begin{aligned}\dot{W}&=\frac{-W-1}{T_1}+\frac{i}{\hbar}\{\vec{\mu}_{21}\cdot\vec{E}(\vec{r},t)\sigma_{12}-\vec{\mu}_{12}\cdot\vec{E}^*(\vec{r},t)\sigma_{21}\},\\ \dot{\sigma}_{21}&=\left(i\Delta-\frac{1}{T_2}\right)\sigma_{21}-\frac{i}{2\hbar}\vec{\mu}_{21}\cdot\vec{E}(\vec{r},t)W,\end{aligned} \tag{14}$$

where $W(\vec{r},t)=\rho_{22}-\rho_{11}$ is the difference between the population probabilities for the upper and lower states. The detuning of the laser frequency, ω_L, from the resonant transition frequency, ω_{21}, of atoms at rest is given by $\Delta=\omega_L-\omega_{21}$. We next expand the dipole moment $\sigma_{21}(\vec{r},t)$ and the population probability difference $W(\vec{r},t)$ in a power series in the phase term of the probe field,

$$\begin{aligned}\sigma_{21}(\vec{r},t)&=\sigma_{21}^{(0)}(\vec{r},t)+\sigma_{21}^{(1)}(\vec{r},t)e^{i\vec{k}_p\cdot(\vec{r}+\vec{v}t)}\\ &\quad+\sigma_{21}^{(-1)}(\vec{r},t)e^{-i\vec{k}_p\cdot(\vec{r}+\vec{v}t)},\\ W(\vec{r},t)&=W^{(0)}(\vec{r},t)+W^{(1)}(\vec{r},t)e^{i\vec{k}_p\cdot(\vec{r}+\vec{v}t)}\\ &\quad+W^{(-1)}(\vec{r},t)e^{-i\vec{k}_p\cdot(\vec{r}+\vec{v}t)}.\end{aligned} \tag{15}$$

When we substitute Eqs. (13) and (15) into (14), and gather terms according to common powers of $e^{i\vec{k}_p\cdot(\vec{r}+\vec{v}t)}$, we arrive at a set of six coupled equations,

$$\begin{aligned}\left(\frac{d}{dt}+\frac{1}{T_2}-i\Delta\right)\sigma_{21}^{(0)}(\vec{r},t)&=-i\{\Omega\cos[\vec{k}_f\cdot(\vec{r}+\vec{v}t)]W^{(0)}(\vec{r},t)\\ &\quad+\Omega_p W^{(-1)}(\vec{r},t)/2\},\end{aligned} \tag{16}$$

$$\begin{aligned}\left(\frac{d}{dt}+\frac{1}{T_2}-i\Delta\right)\sigma_{21}^{(1)}(\vec{r},t)&=-i\{\Omega\cos[\vec{k}_f\cdot(\vec{r}+\vec{v}t)]W^{(1)}(\vec{r},t)\\ &\quad+\Omega_p W^{(0)}(\vec{r},t)/2\},\end{aligned}$$

$$\begin{aligned}\left(\frac{d}{dt}+\frac{1}{T_2}-i\Delta\right)\sigma_{21}^{(-1)}(\vec{r},t)&=-i\Omega\cos[\vec{k}_f\cdot(\vec{r}+\vec{v}t)]\\ &\quad\times W^{(-1)}(\vec{r},t),\end{aligned}$$

$$\begin{aligned}\left(\frac{d}{dt}+\frac{1}{T_1}\right)W^{(0)}(\vec{r},t)&=i[\{2\Omega\cos[\vec{k}_f\cdot(\vec{r}+\vec{v}t)]\sigma_{21}^{(0)*}(\vec{r},t)\\ &\quad+\Omega_p\sigma_{21}^{(1)*}(\vec{r},t)\}\\ &\quad-\{2\Omega^*\cos[\vec{k}_f\cdot(\vec{r}+\vec{v}t)]\sigma_{21}^{(0)}(\vec{r},t)\\ &\quad+\Omega_p^*\sigma_{21}^{(1)}(\vec{r},t)\}]-\frac{1}{T_1},\end{aligned}$$

$$\begin{aligned}\left(\frac{d}{dt}+\frac{1}{T_1}\right)W^{(1)}(\vec{r},t)&=i[\{2\Omega\cos[\vec{k}_f\cdot(\vec{r}+\vec{v}t)]\sigma_{21}^{(-1)*}(\vec{r},t)\\ &\quad+\Omega_p\sigma_{21}^{(0)*}(\vec{r},t)\}\\ &\quad-2\Omega^*\cos[\vec{k}_f\cdot(\vec{r}+\vec{v}t)]\sigma_{21}^{(1)}(\vec{r},t)],\end{aligned}$$

$$\begin{aligned}\left(\frac{d}{dt}+\frac{1}{T_1}\right)W^{(-1)}(\vec{r},t)&=i[2\Omega\cos[\vec{k}_f\cdot(\vec{r}+\vec{v}t)]\sigma_{21}^{(1)*}(\vec{r},t)\\ &\quad-\{2\Omega^*\cos[\vec{k}_f\cdot(\vec{r}+\vec{v}t)]\sigma_{21}^{(-1)}(\vec{r},t)\\ &\quad+\Omega_p^*\sigma_{21}^{(0)}(\vec{r},t)\}].\end{aligned}$$

In these expressions, $\Omega=\vec{\mu}_{21}\cdot\hat{\epsilon}E_f/\hbar$ is the Rabi frequency of the system due to the interaction with the pump beam, and $\Omega_p=\vec{\mu}_{21}\cdot\hat{\epsilon}E_p/\hbar$ is the Rabi frequency of the system due to the probe beam.

The total time- and space-dependent macroscopic polarization induced in the medium is given by

$$\vec{\mathcal{P}}(\vec{r},t)=N\,\mathrm{Tr}(\vec{\mu}\rho)=N(\vec{\mu}_{12}\rho_{21}+\vec{\mu}_{21}\rho_{12}), \tag{17}$$

where N is the density of the atoms in the interaction region. In the laboratory frame, the component of $\vec{\mathcal{P}}(\vec{r},t)$ which radiates into the phase-conjugate wave, is

$$\begin{aligned}\vec{\mathcal{P}}_c(\vec{r},t)&=\tfrac{1}{2}\{\vec{P}_c(\vec{r},t)e^{i[(\vec{k}_f+\vec{k}_b-\vec{k}_p)\cdot\vec{r}-\omega_L t]}\\ &\quad+\vec{P}_c{}^*(\vec{r},t)e^{-i[(\vec{k}_f+\vec{k}_b-\vec{k}_p)\cdot\vec{r}-\omega_L t]}\}\end{aligned} \tag{18}$$

$$=N(\vec{\mu}_{12}\sigma_{21}^{(-1)}e^{i[(\vec{k}_f+\vec{k}_b-\vec{k}_p)\cdot\vec{r}-\omega_L t]}+\text{c.c.}), \tag{19}$$

where P_c is the phasor amplitude of the polarization density. In the slowly varying envelope approximation, the wave equation, which describes the growth of the phase conjugate beam amplitude, E_c, becomes

$$\frac{dE_c}{dz}=\frac{ik_c}{2\epsilon_0}P_c e^{i\Delta\vec{k}\cdot\vec{r}}=\frac{i\omega N\mu_{12}\sigma_{21}^{(-1)}}{c\epsilon_0}e^{i\Delta\vec{k}\cdot\vec{r}}. \tag{20}$$

With careful alignment of the forward and backward pump beams, the conjugate beam is exactly counterpropagating to the probe, and the process is phase matched ($\Delta\vec{k}=0$). Then E_c, found by direct integration of Eq. (20) over the length of the medium L, is

$$E_c=\frac{i\omega N\mu_{12}L\langle\sigma_{21}^{(-1)}\rangle}{c\epsilon_0}, \tag{21}$$

where $\langle\sigma_{21}^{(-1)}\rangle$ is the spatially averaged value of the coherence term, $\sigma_{21}^{(-1)}$, as determined by numerically integrating Eqs. (16). Using the definition of the field attenuation constant, α_0, given by Eq. (2), the phase-conjugate reflectivity is given by

$$R=\frac{I_c}{I_p}=\left|2\alpha_0 L\frac{\gamma_{12}}{\Omega_p}\langle\sigma_{21}^{(-1)}\rangle\right|^2. \tag{22}$$

To carry out the integration of Eqs. (16), we let the transverse relaxation time T_2 be equal to twice the population decay time, T_1, consistent with the collision-free trajectories of the atomic sodium beam. We choose the time interval in the integration to be $T_2/1000$. Longer time intervals start to adversely affect the numerical integration, while shorter intervals would unnecessarily lengthen the computation time. We integrate the optical Bloch equations starting with the Bloch vector $\sigma_{21}=0$ and $W=-1$, i.e., all the population is in the lower state, and the dipole moment is zero. We turn on the field and let the atomic system evolve for $10T_2$ in order to reach equilibrium with the applied optical field.

One check on the validity of the expansion in Eqs. (15) and of this computational technique is to determine the amplitude of the FWM signal for atoms at rest, i.e., $\vec{v}=0$. We can then use the results of Abrams and Lind for a direct quantitative comparison. Since the pump field creates a standing-wave pattern in the medium, the evolution of the atomic system depends upon its location within the field. We therefore carry out the integration at 80 different locations within the standing-wave pattern, spaced by λ/80, for the zero velocity case, and compute $\langle\sigma_{21}^{(-1)}\rangle$ as the simple average of these 80 values of $\sigma_{21}^{(-1)}$. The numerical results, shown in Fig. 4(a) as circles, are in excellent agreement with the Abrams and Lind theory for stationary atoms. We adjust no parameters for either of the curves shown in Fig. 4. We start to see some anomalies in our results at $I=350$ mW/cm^2 (off scale in Fig. 4), presumably due to the high Rabi frequency of the pump. This may be due to either of the two following reasons. The standing-wave pattern of the electric field is sufficient to strongly saturate the transition of the two-level system everywhere except for the small volume surrounding the nodes of the electric field. Since the maximum FWM signal is generated for $I\sim I_{\rm sat}^0$, our analysis of the oscillating dipole at 80 equally spaced locations within the standing wave may miss some of important contributions to the signal. Also, as the Rabi frequency increases, the period of the rapid oscillation of the Bloch vector may be too short for the numerical integration to follow. We believe the former to be the case, as we observe an improvement in the results when we increase the number of points within the standing wave pattern. In either case, we limit the calculations of the FWM intensity to pump intensities less than $60I_{\rm sat}^0$, a value well in excess of the intensities we can achieve in our experiments.

For the atoms with nonzero transverse velocity, their motion over the standing-wave pattern lets them sample the full range of electric field amplitudes, and we find there is no need to distinguish between different starting locations within the standing-wave pattern. Their motion effectively modulates the pump field at a frequency $\vec{k}\cdot\vec{v}$, leading to periodic evolution of the population difference W and the dipole σ. Our numerical results show that $\sigma_{21}^{(0)}$, $W^{(+1)}$, and $W^{(-1)}$ all undergo modulation at odd integer multiples of $\vec{k}\cdot\vec{v}$, while $\sigma_{21}^{(+1)}$, $\sigma_{21}^{(-1)}$, and $W^{(0)}$ display modulation at even integer multiples of $\vec{k}\cdot\vec{v}$. We show $\sigma_{21}^{(-1)}$ as a function of time for $\vec{k}\cdot\vec{v}=0.2/T_2$ (dot-dashed line) and $\vec{k}\cdot\vec{v}=0.6/T_2$ (solid line), and $\Omega=0.1/T_2$ in Fig. 5. This signal takes a few cycles to reach steady state, after which it shows sinusoidal modulation at frequency $2\vec{k}\cdot\vec{v}$ about an average nonzero level. At larger Rabi frequencies, additional Fourier components at higher even multiples of $\vec{k}\cdot\vec{v}$ show up as well. We can write the dipole moment as

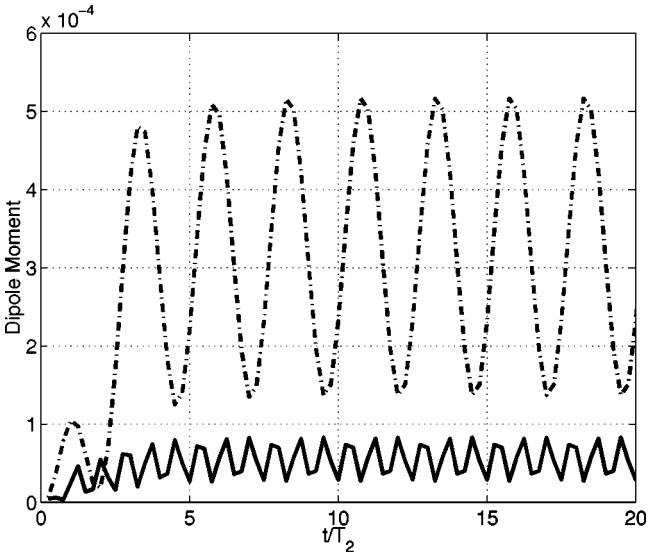

FIG. 5. Modulation of $\sigma_{21}^{(-1)}$ as the atom travels across the standing-wave pattern formed by the counterpropagating pump beams. The intensity of the pump beams corresponds to a Rabi frequency of $\Omega=0.1/T_2$. The dot-dashed line is for $\vec{k}\cdot\vec{v}=0.2/T_2$, while the solid line is for $\vec{k}\cdot\vec{v}=0.6/T_2$.

$$\sigma_{21}^{(-1)}=\sigma_0+\sigma_2\sin(2\vec{k}\cdot\vec{v}t+\phi_2)+\sigma_4\sin(4\vec{k}\cdot\vec{v}t+\phi_4)+\cdots, \tag{23}$$

where the coefficients σ_i depend upon the velocity of the atoms and the Rabi frequency, Ω. The phases, ϕ_i, depend on the starting point for each individual atom, and are randomly distributed over 2π.

The radiated signal is proportional to the time-averaged square of the spatial average of the dipole moments,

$$|\langle\sigma_{21}^{(-1)}\rangle|^2=\overline{\left(\frac{1}{NV}\sum_{\text{all atoms}}\sigma_{21}^{(-1)}\right)^2}=\overline{\left(\sum_{v,\phi_i}g(v)\sigma_{21}^{(-1)}\right)^2}, \tag{24}$$

where $g(v)$ is the distribution function of the transverse velocities, as defined earlier, and the overbar represents the time average. Since the ϕ_i are randomly distributed, only the average terms survive, and

$$|\langle\sigma_{21}^{(-1)}\rangle|^2=\left(\sum_v g(v)\sigma_0(v)\right)^2. \tag{25}$$

In Fig. 6, we show a plot of the σ_0 as a function of $\vec{k}\cdot\vec{v}$ for four different values of ΩT_2. At low intensities, the average intensity of the FWM signal drops off rapidly with increasing $\vec{k}\cdot\vec{v}$. As an example, for atoms whose transverse velocity is $v=0.2\lambda/2\pi T_2$, which is only 60 cm/sec for this transition

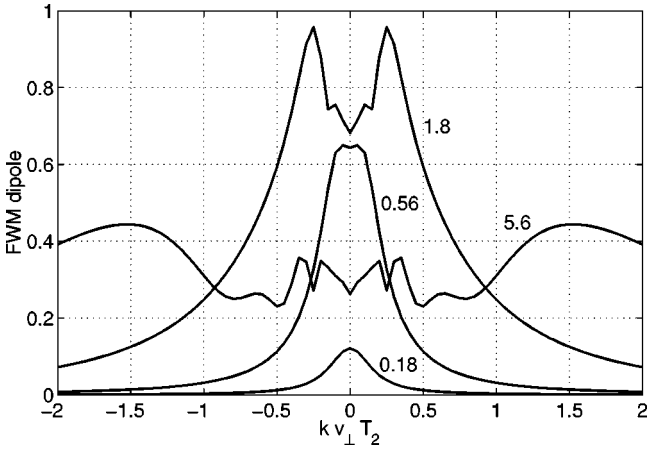

FIG. 6. Average value of the coherence term that radiates the phase-conjugate wave $\sigma_0(v)$ as a function of the transverse atomic velocity. The pump beam field amplitude, shown as the product ΩT_2, is given for each curve.

in sodium, the dipole moment that radiates the phase-conjugate field is already decreased to 40% of that for the $v=0$ atoms. Since the full width of the velocity distribution of the atomic beam is ~ 300 cm/sec, we can see that a significant fraction of the atoms do not contribute to the signal. At increased intensity, however, the dipole response of the atoms is power broadened, so that atoms with larger velocities can still contribute to the FWM signal. This behavior is clearly seen in Fig. 6. In fact, the peak of these curves shifts to larger velocities as the intensity is increased. This shift results in a FWM signal in Doppler-broadened media which is actually increased over that for a zero-velocity medium.

We show the results of Eqs. (22) and (25) as the dashed line in Fig. 4(a). We have used a Doppler width of 8 MHz (FWHM) to best fit our data in this curve. This is somewhat larger than the 5 MHz width we determined by deconvolving our absorption spectrum, but still within a range we consider reasonable. An 8-MHz Doppler width results in an absorption spectrum whose width is 14.5 MHz FWHM. Factors that could account for this discrepancy include: (i) our assumption of a Gaussian shape for $g(v)$ for our calculations, (ii) the uncertainty in the measured width of the absorption spectrum, and iii) the uncertainty in the FWM peak heights. Overall, the agreement of the data with the Doppler-modified curve is very reasonable.

We also expect that the transverse velocities of the atoms can help to explain the small deviation at low intensities between measured linewidths of the FWM spectra and those expected on the basis of Eq. (5). We have not carried out any calculations to support this claim, but expect that for small transverse velocity, the atomic response is increased for slight detunings of the laser from resonance. Thus the linewidth of the FWM interaction is increased due to the Doppler-shifted resonance enhancement of these atoms. At larger intensities, the atomic response is power broadened, and the Doppler shift has little influence on the linewidth.

V. CONCLUSIONS

The measurements we have made of the power of the FWM signal as a function of the pump intensity show excellent overall agreement with the Abrams and Lind theory, modified to include the transverse velocity effects present in our atomic beam system. Measurements of the bandwidth of the experimental FWM signal agree well with the theoretical result for large pump intensities, but are slightly greater for pump intensities less than I_{sat}. This we attribute to the atomic velocities as well, since the Doppler effect will slightly broaden the spectrum at low intensities, but not at high intensities where the atomic response is power broadened, and less dependent on the atomic velocity. We find it surprising that the atomic velocity has such a pronounced effect on the saturation characteristic of this interaction. Close agreement between our experimental and numerical results, however, is very convincing. These experimental results provide direct quantitative confirmation of the fundamental theory for phase-conjugate four-wave mixing in a resonant absorbing medium.

ACKNOWLEDGMENTS

We are grateful for a useful conversation with Duncan Steel concerning these results, for help from Scott DeMange with fitting the spectra, and for preliminary work at the initiation of this project by Mike Anderson and Ce Chen. This material is based upon work supported by the U.S. Army Research Office under Grant No. DAAH04-95-1-0361. We also acknowledge the support of the NSF in the early stages of the work carried out at JILA.

[1] Thomas R. O'Meara, David M. Pepper, and Jeffrey O. White, in *Optical Phase Conjugation*, edited by Robert A. Fisher (Academic Press, San Diego, 1983), Chap. 14.

[2] A. E. Siegman, Pierre A. Belanger, and Amos Hardy, in *Optical Phase Conjugation* (Ref. [1]), Chap. 13.

[3] David M. Pepper, John AuYeung, Dan Fekete, and Amnon Yariv, Opt. Lett. **3**, 7 (1978).

[4] Ivan Giaggio, Jouni P. Partanen, B. Ai, R. J. Knize, and Robert W. Hellwarth, Nature (London) **371**, 318 (1994).

[5] Joseph Nilsen, Natalie S. Gluck, and Amnon Yariv, Opt. Lett. **6**, 380 (1981).

[6] P. F. Liao, D. M. Bloom, and N. P. Economou, Appl. Phys. Lett. **32**, 813 (1978).

[7] P. Aubourg, J. P. Bettini, G. P. Agrawal, P. Cottin, D. Guérin, O. Meunier, and J. L. Boulnois, Opt. Lett. **6**, 383 (1981).

[8] J. G. Coffer, R. A. Chodzko, J. M. Bernard, and H. Mirels, Appl. Phys. Lett. **56**, 1524 (1990).

[9] Michael S. Brown, Larry A. Rahn, and Thomas Dreier, Opt. Lett. **17**, 76 (1992).

[10] P. Ewart and P. Snowdon, Opt. Lett. **15**, 1403 (1990).

[11] Geoffrey J. Germann, Roger L. Farrow, and David J. Rakestraw, J. Opt. Soc. Am. B **12**, 25 (1995).

[12] Peter Ljungberg and Ove Axner, Appl. Opt. **34**, 527 (1995).
[13] A. Klamminger, M. Motzkus, S. Lochbrunner, G. Pichler, K. L. Kompa, and P. Hering, Appl. Phys. B: Lasers Opt. **61**, 311 (1995).
[14] C. J. Gaeta, J. F. Lam, and R. C. Lind, Opt. Lett. **14**, 245 (1989).
[15] M. Oria, D. Bloch, M. Fichet, and M. Ducloy, Opt. Lett. **14**, 1082 (1989).
[16] M. Pinard, R. Horowicz, D. Grandclément, and G. Grynberg, IEEE J. Quantum Electron. **25**, 570 (1989).
[17] D. Grandclément, M. Pinard, and G. Grynberg, IEEE J. Quantum Electron. **25**, 580 (1989).
[18] C. J. Gaeta and David M. Pepper, Opt. Lett. **16**, 802 (1991).
[19] R. E. Slusher, L. W. Hollberg, B. Yurke, J. C. Mertzw, and J. F. Valley, Phys. Rev. Lett. **55**, 2409 (1985); **56**, 788 (1986).
[20] R. L. Abrams and R. C. Lind, Opt. Lett. **2**, 94 (1978); **3**, 205 (1978).
[21] R. L. Abrams, J. F. Lam, R. C. Lind, D. G. Steel, and P. F. Liao, in *Optical Phase Conjugation* (Ref. [1]), Chap. 8.
[22] Binh Do, Jongwhan Cha, D. S. Elliott, and S. J. Smith (unpublished).
[23] S. M. Wandzura, Opt. Lett. **4**, 208 (1979).
[24] D. G. Steel and R. C. Lind, Opt. Lett. **6**, 587 (1981).
[25] J. F. Lam, D. G. Steel, R. A. McFarlane, and R. C. Lind, Appl. Phys. Lett. **38**, 977 (1981).
[26] Martial Ducloy, Fernando A. M. de Oliveira, and Daniel Bloch, Phys. Rev. A **32**, 1614 (1985).
[27] Sylvie Le Boiteux, Pierre Simoneau, Daniel Bloch, Fernando A. M. de Oliveira, and Martial Ducloy, IEEE J. Quantum Electron. **22**, 1229 (1986).
[28] Cláudio L. Cesar, José W. R. Tabosa, Paulo C. de Oliveira, Martial Ducloy, and José R. Rios Leite, Opt. Lett. **13**, 1108 (1988).
[29] Thomas A. Reichardt and Robert P. Lucht, J. Opt. Soc. Am. B **13**, 1107 (1996).
[30] See, for example, L. Allen and J. H. Eberly, *Optical Resonance and Two-Level Atoms* (John Wiley, New York, 1975).
[31] R. E. Grove, F. Y. Wu, and S. Ezekial, Phys. Rev. A **15**, 227 (1977).
[32] Norman F. Ramsey, *Molecular Beams* (Oxford University Press, Oxford, 1955), Sec. II.2.
[33] A. N. Nesmeyanov, *Vapour Pressure of the Elements* (Academic Press, New York, 1963).
[34] R. V. Pound, Rev. Sci. Instrum. **17**, 490 (1946).
[35] R. W. P. Drever, J. L. Hall, F. V. Kowalski, J. Hough, G. M. Ford, A. J. Munley, and H. Ward, Appl. Phys. B: Photophys. Laser Chem. **31**, 97 (1983).
[36] V. I. Balykin, V. S. Letokhov, V. G. Minogin, Yu. V. Rozhdestvensky, and A. I. Sidorov, J. Opt. Soc. Am. B **2**, 1776 (1985).
[37] R. E. Scholten, R. Gupta, J. J. McClelland, R. J. Celotta, M. S. Levenson, and M. G. Vangel, Phys. Rev. A **55**, 1331 (1997).
[38] Pierre Meystre and Murray Sargent III, *Elements of Quantum Optics* (Springer, Berlin, 1991), 2nd ed., Sec. 6.3.